Atmospheric Environment 339 (2024) 120890

Contents lists available at ScienceDirect

Atmospheric Environment

journal homepage: www.elsevier.com/locate/atmosenv

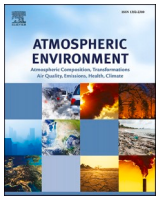

Elucidating the impacts of aerosol radiative effects for mitigating surface O_3 and $PM_{2.5}$ in Delhi, India during crop residue burning period

Lakhima Chutia [a,b], Jun Wang [a,b,*], Huanxin Zhang [a,b], Xi Chen [a,b], Lorena Castro Garcia [a,b], Nathan Janechek [b]

[a] Department of Chemical and Biochemical Engineering, College of Engineering, University of Iowa, IA, USA
[b] Iowa Technology Institute and Global and Regional Environmental Research, College of Engineering, University of Iowa, IA, USA

HIGHLIGHTS

- The aerosol–photolysis effect (APE) reduces surface O_3 and $PM_{2.5}$ concentration in Delhi during post-monsoon period.
- APE and Aerosol Radiative Feedback (ARF) notably influence O_3 and $PM_{2.5}$ levels from smoke during crop residue burning period.
- Control of urban VOC helps both O_3 and $PM_{2.5}$ reductions in Delhi, even after considering biomass burning emissions.

ARTICLE INFO

Keywords:
Indian air quality
O_3
$PM_{2.5}$
Crop residue burning
Aerosol radiative effects
Photolysis

ABSTRACT

Atmospheric aerosol radiative effects regulate surface air pollution (O_3 and $PM_{2.5}$) via both the aerosol–photolysis effect (APE) and the aerosol–radiation feedback (ARF) on meteorology. Here, we elucidate the roles of APE and ARF on surface O_3 and $PM_{2.5}$ in the heavily polluted megacity, Delhi, India by using a regional model (WRF-Chem) with constraints from limited surface observations. While APE reduces surface O_3 (by 6.1%) and $PM_{2.5}$ concentrations (by 2.4% via impeding the secondary aerosol formations), ARF contributes to a 2.5% and 17.5% increase in surface O_3 and $PM_{2.5}$, respectively. The ARF from smoke enhances $PM_{2.5}$ (by 8%), black carbon (by 10%), and primary organic aerosol (by 18%) during late autumn when crop residue burning is significant. The synergistic APE and ARF have a negligible impact on the total concentrations of O_3 and $PM_{2.5}$. Hence, the reduction of $PM_{2.5}$ may lead to O_3 escalation due to weakened APE. Sensitivity experiments indicate the need and effectiveness of reducing VOC emission for the co-benefits of mitigating both O_3 and $PM_{2.5}$ concentrations in Delhi.

1. Introduction

Ground-level ozone (O_3) and fine particulate matter with aerodynamic diameter $\leq$2.5 μm ($PM_{2.5}$) are dominant air pollutants in megacities such as Delhi, India. Delhi has been experiencing severe air pollution episodes in recent years, especially during the post-monsoon (Oct.–Nov.) and winter (Dec.–Feb.) seasons associated with crop residue burning and widespread winter haze, respectively (Bharali et al., 2019; Kumar et al., 2020; Saxena et al., 2021). Crop residue burning typically occurs twice a year, mostly in northwest India, after rice harvests in October–November and wheat harvests in April–May (pre-monsoon) – providing farmers with a quick and cost-effective method for clearing fields for the next cropping season (Lan et al., 2022). This practice has particularly severe effects during the post-monsoon season, exacerbated by limited dispersion due to inversion conditions, which spreads across northern India, including Delhi, resulting in critical levels of $PM_{2.5}$ and O_3 (Singh et al., 2023). Despite government bans and advisories, crop burning remains widespread due to socioeconomic factors, limited awareness of its harmful effects, and the financial advantages over alternative methods (Bhuvaneshwari et al., 2019; Lan et al., 2022). Both $PM_{2.5}$ and O_3 concentrations often exceed Indian National Ambient Air Quality Standards, posing a serious threat to public health (Jat et al., 2021; Nelson et al., 2021; Sahu and Kota, 2017), leading to ~ 1 million and 31,000 premature deaths per year in India, respectively (Conibear et al., 2018; Ghude et al., 2016). Besides, O_3 and $PM_{2.5}$ exposure damages crops and significantly reduces wheat and rice (22–42%) yields in

* Corresponding author. Department of Chemical and Biochemical Engineering, College of Engineering, University of Iowa, IA, USA.
E-mail address: jun-wang-1@uiowa.edu (J. Wang).

https://doi.org/10.1016/j.atmosenv.2024.120890
Received 19 December 2023; Received in revised form 13 October 2024; Accepted 21 October 2024
Available online 22 October 2024

India (Sinha et al., 2015). Therefore, the prediction and process understanding of both $PM_{2.5}$ and O_3 are highly essential to improve the air quality and mitigate their impacts on public health and agriculture in this region.

Past studies have focused on several factors including emission, meteorology, and atmospheric chemistry governing the high concentrations of $PM_{2.5}$ and O_3 in the Indian region (e.g., Bran and Srivastava, 2017; Ojha et al., 2020). One factor often overlooked in the literature is the impacts of aerosol–radiation interaction (ARI) on both $PM_{2.5}$ and O_3 and the non-linear synergistic processes therein. The ARI influences O_3 chemistry and atmospheric oxidation capacity by modulating photolysis rates in the troposphere, known as the aerosol–photolysis effect (APE). This process further influences the particle formation process and air quality (Benas et al., 2013; Li et al., 2011). Modeling studies have highlighted the reduction in photolysis rate (e.g., NO_2 and O_3 photolysis rates) due to the strong absorption of aerosols (Liao et al., 1999; Tie et al., 2003), with subsequent effects on the O_3 formation. Several studies have analyzed the impact of APE in different parts of the world such as the urban environment in China (Xing et al., 2017; Yang et al., 2022), Mexico (Li et al., 2011), Europe (Real and Sartelet, 2011), and Texas (Flynn et al., 2010). However, such studies are limited over the Indian region, especially during the months of crop residue burning.

ARI not only entails APE but also includes aerosol–radiation feedback (ARF) on meteorology that in turn affects surface O_3 and aerosol distribution. ARF can lead to a substantial decrease in solar radiation reaching the ground, thereby reducing surface temperature and the planetary boundary layer (PBL) height. Via absorption of radiation, aerosols can heat the atmosphere, increase atmospheric stability, and further enhance aerosol concentration in the PBL; this positive feedback via ARF is particularly significant during severe pollution episodes (Liu et al., 2018; Wang et al., 2020). A recent study by Yang et al. (2022) investigated APE and ARF effects focusing on O_3 during extreme air quality episodes in pre-monsoon months in Northern China, whereas Wu et al. (2020) focused on $PM_{2.5}$ during winter pollution events. However, these studies did not explore the synergistic (or confounding) impacts of ARF and APE for both O_3 and $PM_{2.5}$. Furthermore, the findings from the extreme haze events, as conducted in aforementioned studies in China, might not fully address the prevailing conditions in Delhi, which is affected not only by local emissions but also by the emissions from crop residue burning in neighboring areas - one of the uniqueness that distinguishes the air pollution problems in Delhi from other megacities in East Asia.

Here we employ a regional chemistry transport model (WRF-Chem) to elucidate the relative impact of APE and ARF and study their implications for simultaneously mitigating surface $PM_{2.5}$ and O_3 in the National Capital Region (NCR) of India. WRF-Chem has been widely used for the simulation of $PM_{2.5}$ and O_3 across the Indian region (e.g., Mogno et al., 2021; Sharma et al., 2017). But only a few studies have focused on the impacts of ARF (Bharali et al., 2019; Kumar et al., 2020) with no study analyzing the pure and synergistic effect of APE and ARF. Kumar et al. (2020) showed that the inclusion of ARF in WRF-Chem can lead to a significant improvement in $PM_{2.5}$ forecast by reducing the mean bias up to 25% in NCR Delhi. Mukherjee et al. (2020) found a 30% reduction in surface O_3 concentration due to APE associated with black carbon (BC) over South Asia. Hence, while reducing BC may lead to a decrease in $PM_{2.5}$, it may lead to an increase in surface O_3 concentration. While the earlier studies explored these individual aspects, our study is unique in several key aspects. First, we aim to capture a broader picture of APE and ARF effects by focusing on both $PM_{2.5}$ and O_3 over Delhi during the post-monsoon period when crop residue burning occurs. Second, our study takes a unique approach by elucidating the synergistic APE and ARF impacts that were not studied previously. The scientific consideration of the role of both APE and ARF and their synergistic effects is essential for the air pollution mitigation strategy, and their overall net effects across the Indian region would remain elusive without a quantitative study. Third, to quantify these impacts, we employ the factor separation approach (FSA) method (see section 2.2) introduced by Stein and Alpert (1993), a distinct methodology from the earlier works. Moreover, our study fills the gap of studies in understanding the ARI processes during the crop residue burning period by accounting these effects from the fire emissions.

The contributions of APE and ARF are quantitatively analyzed here through model sensitivity simulations with the constraint of surface observations (described in section 2.3), focusing on the crop residue burning period in November 2018 over NCR Delhi. Results are presented in Section 3, starting from the comparison of the model results with observations (Section 3.1) to the analysis of the impact of pure and synergistic APE and ARF and their impact from fire emissions (Section 3.2–3.4) and discussions (Section 3.5). The summary and conclusions are provided in Section 4.

2. Methodology

2.1. Model description

A regional model with Unified Inputs (of initial and boundary conditions) for the Weather Research and Forecasting model coupled with chemistry (UI-WRF-Chem) (Fast et al., 2006; Grell et al., 2005; Wang et al., 2023) is used to simulate O_3 and $PM_{2.5}$ in Delhi in two nested domains at 12 and 4 km horizontal resolutions, respectively. The outer and inner domains cover the entire northern Indian subcontinent and NCR Delhi, respectively (Fig. 1). There are 47 vertical layers from the ground to 50 hPa. The UI-WRF-Chem model utilizes Modern-Era Retrospective Analysis for Research and Applications, Version 2 (MERRA-2) data to provide both meteorological and chemical initial and boundary conditions. Initial conditions for soil properties are taken from the Global Land Data Assimilation System (GLDAS) at a horizontal resolution of $0.25^\circ \times 0.25^\circ$.

The WRF-Chem emission preprocessing system (WEPS) designed in-house is used to prepare the anthropogenic and biogenic emissions needed for UI-WRF-Chem (Sha et al., 2021; Wang et al., 2023). Anthropogenic emissions are based on the Emissions Database for Global Atmospheric Research - Hemispheric Transport of Air Pollution (HTAPv2; Janssens-Maenhout et al., 2015) which includes PM_{10}, $PM_{2.5}$, BC, OC, NH_3, NMVOCs, CO, NOx and SO_2 at a horizontal resolution of $0.1^\circ \times 0.1^\circ$. Biomass burning emissions from the Fire Locating and Modeling of Burning Emissions Inventory (FLAMBE; Reid et al., 2009) is used to specify the sources of BC, OC, and gaseous species (CO, NO_2) as a function of time. Further details of FLAMBE and WEPS can be found elsewhere (Ge et al., 2017; Wang et al., 2013). Regional Acid Deposition Model version 2 (RADM2) (Stockwell et al., 1990) coupled with the Modal Aerosol Dynamics for Europe (MADE) and the Secondary Organic Aerosol Model (SORGAM) (Schell et al., 2001) are used to simulate the gas-phase chemistry and aerosols. Our choice of the RADM2 mechanism was based on the findings of Sharma et al. (2017) and other relevant literature on gas and aerosol simulations using the WRF-Chem model over the Indian region, such as studies by Chutia et al. (2019) and Girach et al. (2017). Sharma et al. (2017) investigated the sensitivity of modeled O_3 using both the MOZART and RADM2 mechanisms with HTAPv2 emissions, which we also employed in this study, and found comparable performance between the two mechanisms. HTAP-MOZART yielded higher noontime surface O_3 with a normalized mean bias value of ~34.2%, compared to ~20.9% for HTAP-RADM2 over Indian region (Sharma et al., 2017). Additionally, the inorganic chemistry system considered in MADE is currently limited to sulfate, nitrate, ammonium, and water components in the aerosol phase. The Fast Tropospheric UV and Visible Radiation Model (FTUV) (Li et al., 2005) is used to evaluate aerosol effects on photolysis rates and the Goddard shortwave radiative transfer module (Chou and Suarez, 1994) is employed for estimating shortwave radiation. Other physics parameterization schemes (Table S1) used here are based on the earlier studies using the WRF-Chem model over the Indian region (Chutia et al., 2019; Ojha et al.,

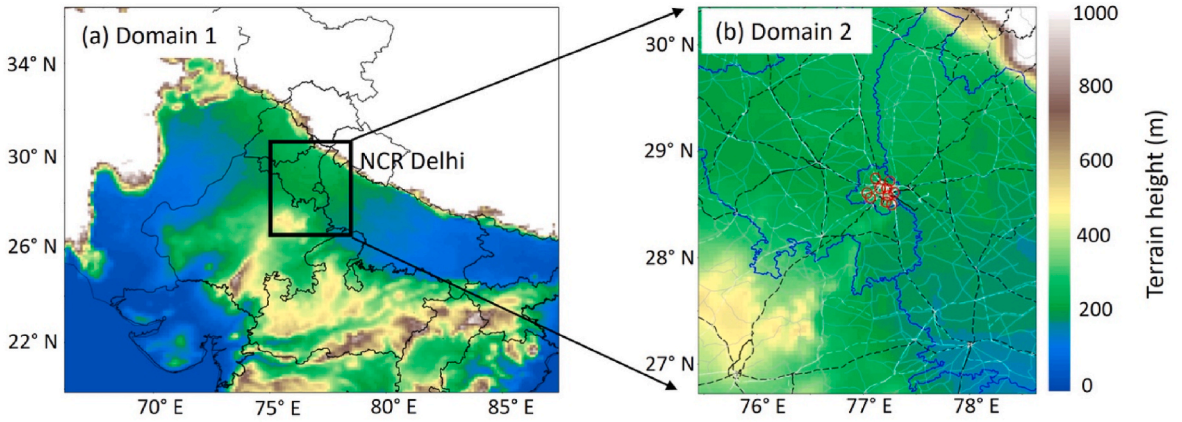

Fig. 1. Simulation domains showing terrain height (meter). **(a)** Domain 1 covers the Northern Indian subcontinent at 12 km resolution **(b)** Domain 2 covers NCR Delhi at 4 km resolution. Red circles represent the observation sites, the dashed black and grey lines represent national highways and other roads, the white dashed lines represent railways, and the solid blue lines show the state boundaries.

2020).

2.2. Simulation scenarios and analysis method

We utilized the factor separation approach (FSA) method (Stein and Alpert, 1993) to obtain the pure contribution of APE and ARF and their synergistic contributions due to the mutual interactions among APE and ARF. Based on the FSA, four simulations called AFRP (Anthro--Fire-Radiation-Photolysis), AFR_0P_0, $AFRP_0$, and AFR_0P, have been performed to quantify the pure and synergistic impacts of APE and ARF on O_3 and $PM_{2.5}$ (See Table 1). Subscript 0 denotes that the corresponding effect is turned off. In the AFRP simulation, the impacts of both ARF and APE are considered. In AFR_0P_0, both ARF and APE are turned off, and in $AFRP_0$, and AFR_0P, only ARF and APE are considered respectively. In all these simulations, anthropogenic and fire emissions are turned on.

Considering that $f_{ARF+APE}$, f_{ARF}, f_{APE}, and f_0 are the simulation results including both APE and ARF (experiment AFRP), only ARF, and APE (experiment $AFRP_0$, and AFR_0P), and neither APE nor ARF (experiment AFR_0P_0), respectively, one can show the synergistic contributions between APE and ARF as follows:

$$f'_{ARF+APE} = f_{ARF+APE} - f_{APE} - f_{ARF} + f_0 \quad \text{(i)}$$

Further, to investigate the impact of APE and ARF from fire emissions we have performed three more simulations: AF_0RP (no fire emission); AF_0R_0P (fire emission and ARF turned off), and AF_0RP_0 where fire emission and APE are turned off (Table 1). The fire impact on APE and ARF is estimated using the below equations

$$\text{Contribution of APE from fire} = (AFRP - AFRP_0) - (AF_0RP - AF_0RP_0) \quad \text{(ii)}$$

$$\text{Contribution of ARF from fire} = (AFRP - AFR_0P) - (AF_0RP - AF_0R_0P) \quad \text{(iii)}$$

Each simulation is performed from 22 October to 30 November 2018 with the first 10 days as the model spin up.

Table 1
UI-WRF-Chem experiments performed in the study.

Sl No	Exp	Anthro	Fire	Radiation	Photolysis
1	AFRP	ON	ON	ON	ON
2	AFR_0P_0	ON	ON	OFF	OFF
3	$AFRP_0$	ON	ON	ON	OFF
4	AFR_0P	ON	ON	OFF	ON
5	AF_0RP	ON	OFF	ON	ON
6	AF_0R_0P	ON	OFF	OFF	ON
7	AF_0RP_0	ON	OFF	ON	OFF

2.3. Observational data

Ground-based measurements of $PM_{2.5}$, O_3, and meteorological parameters (temperature and relative humidity) at different stations over NCR Delhi (Fig. 1b and Table S2) for the period of November 2018 are obtained from the Central Pollution Control Board (CPCB), India. The instruments are periodically calibrated, and measurements are regularly checked and controlled with quality assurance by the CPCB (cpcb.nic.in/quality-assurance-quality-control/) (CPCB, 2018; Singh et al., 2021). Additional data assurance is considered by removing very high (>1500 μg m^{-3}) and low (<10 μg m^{-3}) $PM_{2.5}$ values following Kumar et al. (2020). For O_3 data filtering, we excluded days with abnormally low O_3 values during daytime hours, as well as data points with constant O_3 values over extended periods or showing abrupt variations. Furthermore, we ensured that the selected data reflected the typical diurnal pattern of O_3 concentrations in the urban environment.

3. Results

3.1. Model evaluation

The AFRP and AFR_0P_0 simulations are first used for the evaluation of the overall impact of ARI on the model results. The diurnal pattern and magnitude of 2 m air temperature (T2) and relative humidity (RH) are captured well by the UI-WRF-Chem in both simulations, with a relatively smaller bias in the AFRP case (Fig. 2a and b and Table S3). The normalized mean bias (NMB) between the observation and model is reduced from −11% in AFR_0P_0 to −5% in AFRP for RH and 5% to 2% for T2.

Fig. 2(c and d) illustrate the monthly averaged diurnal variation of observed and simulated surface $PM_{2.5}$ and O_3 concentrations in megacity Delhi during November 2018. The average observed $PM_{2.5}$ concentration in Delhi is 156.7 μg m^{-3}, with modeled values of 155 μg m^{-3} and 138 μg m^{-3} in the AFRP and AFR_0P_0 simulations, respectively, all exceeding the WHO daily guideline of 15 μg m^{-3} (WHO, 2021) by 9 to 10 times. While the figure shows the diurnal variation of O_3, the observed maximum 8-h mean O_3 concentration is 83 ppb, with modeled values of 102 ppb and 110 ppb in the AFRP and AFR_0P_0 simulations, respectively, which are about 1.5 to 2 times higher than the WHO guideline of ~51 ppb (100 μg m^{-3}). The UI-WRF-Chem captured the observed diurnal variations of surface O_3 and $PM_{2.5}$ with a good correlation (of 0.96–0.97 and 0.52–0.62, respectively) in both AFRP and AFR_0P_0 simulations (Fig. 2c and d and Table S3). However, the model overestimates the daytime O_3 peak in both simulations (MB of 16 ppb in the AFR_0P_0 case), with relatively less bias in the AFRP case (MB of 11

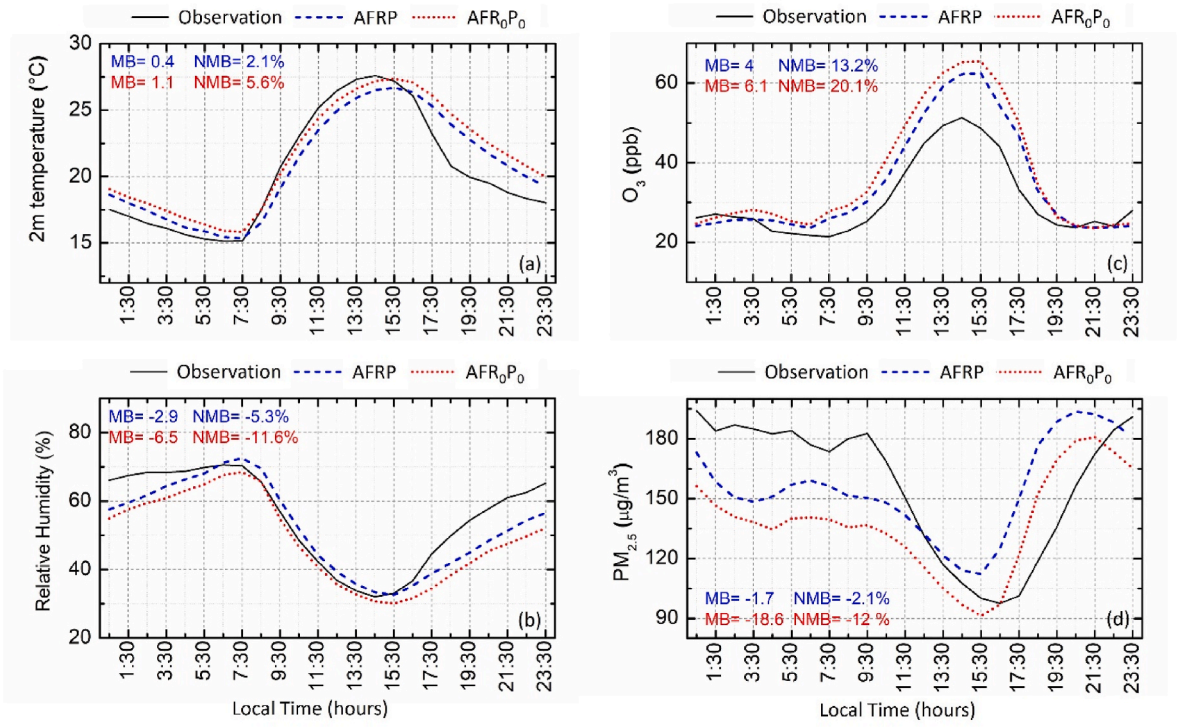

Fig. 2. Diurnal variation of observed (black) and simulated variables (blue for AFRP and red for AFR_0P_0 experiments). **(a)** 2m temperature (° C), **(b)** relative humidity (%), **(c)** O_3 (ppb), and **(d)** $PM_{2.5}$ (μg m^{-3}) in megacity Delhi during November 2018.

ppb). Additionally, the peak of the observed $PM_{2.5}$ mass related to the morning rush hour traffic emissions is not captured well by the UI-WRF-Chem. Nevertheless, the modeled correlation of diurnal variation with observation has coefficients of 0.52–0.62. The differences between the model and observation could be associated with uncertainties in the input emissions, boundary layer processes, meteorology, and chemical processes. Furthermore, the absolute levels of O_3 and $PM_{2.5}$ simulated here are also consistent with the earlier model-based studies in this region (Hakim et al., 2019; Ojha et al., 2020). However, the model performed better in the AFRP experiment i.e., when both the APE and ARF are considered. The overall NMB between the model and observed O_3 is reduced from 20% in AFR_0P_0 to 13% in the AFRP experiment. Similarly, the NMB decreased from 12% in AFR_0P_0 to 2% in the AFRP simulation for $PM_{2.5}$. This supports previous findings by Kumar et al. (2020) where they reported that ARF can lead to ~21–25% reduction in the mean bias of the $PM_{2.5}$ forecast in Delhi; however, the APE effects on O_3 and synergistic APE and ARF effects were not quantified in their study. The contrast between AFRP and AFR_0P_0 suggests the need to consider both the role of APE and ARF toward the improvement of UI-WRF-Chem simulation of surface O_3 and $PM_{2.5}$.

3.2. Pure contribution of APE and ARF

Fig. 3(b, c, f, g, j, k) and Table 2 illustrate the pure contribution of APE and ARF on surface O_3, NO_2, and $PM_{2.5}$ concentrations over NCR Delhi. The pure APE contributed to a reduction in the O_3 concentration by 3.29 ppb (6.1%) via weakening the efficiency of the photolytic reaction. In the pure APE scenario, the surface photolysis rates $J[NO_2]$ and $J[O^1D]$ are decreased by ~23% over NCR Delhi (Figs. S1a and d, Table 2), which in turn reduces the surface O_3 and OH radical concentration (Fig. S1g). The reduction in $J[NO_2]$ and $J[O^1D]$ is particularly significant (Fig. S2) during the early morning (07:30–08:30 LT) and late afternoon hours (15:30–16:30 LT, i.e., when the solar zenith angle is at around 60°), signifying the influence of long path length of aerosol optical extinction for incoming ultraviolet radiation. In contrast, the pure impact of ARF increases surface O_3 over most areas of the simulated domain by up to 3 ppb but slightly decreases in the megacity Delhi by up to 0.5 ppb. Overall ARF increases the surface O_3 by 2.5% over the entire simulated domain (Fig. 3c), primarily due to the reduction of the PBL height and surface energy budget by ARF. The aerosol-induced solar dimming (−47 Wm^{-2}) leads to a cooling of –1K at the surface and decreases the surface wind speed (−0.11 ms^{-1}) and noontime boundary layer height by ~143 m over the simulated domain (Fig. 4). The reduced ventilation due to the shallower atmospheric boundary layer and weaker winds caused by the ARF enhances the precursor levels resulting in greater O_3 chemical formation. Contrarily, in megacity Delhi, which is a VOC-limited regime (Nelson et al., 2021), increased NO_2 (Fig. 3g) concentrations at the surface associated with the ARF inhibit O_3 formation due to the enhanced titration by NO, although this O_3 reduction due to ARF in megacity Delhi is far less significant than the changes caused by APE.

In the case of $PM_{2.5}$, pure ARF contributes substantially to the $PM_{2.5}$ accumulation near the surface with an average contribution of 17.5% (16.8 μg m^{-3}) over the simulated domain (Fig. 3k). The increased atmospheric stability due to pure ARF hinders the $PM_{2.5}$ dispersion and subsequently aggravates $PM_{2.5}$ pollution near the surface. On the other hand, pure APE inhibits the $PM_{2.5}$ concentrations and leads to a decrease of 2.4% (2.29 μg m^{-3}). To corroborate this finding, changes in the secondary inorganic aerosols such as sulfate, nitrate, and ammonium (SNA) in pure ARF and APE scenarios are analyzed (Fig. S3). Bawase et al. (2021) reported that SNA ions (31.44 ± 20.69 μg m^{-3}) are one of the largest contributors to $PM_{2.5}$ along with organic matter in Delhi. As seen in Fig. S3 and Table 2, pure ARF substantially enhances the surface SNA concentration while pure APE leads to a slight reduction. On average, sulfate, nitrate, and ammonium concentrations are increased by 0.26 μg m^{-3} (6.1%), 10.4 μg m^{-3} (25.9%), and 3.1 μg m^{-3} (23%), respectively due to pure ARF. The extent of SNA changes due to APE is relatively smaller than the changes caused by the pure ARF effect. Pure APE decreases sulfate, nitrate, and ammonium concentration by 0.25 μg m^{-3}

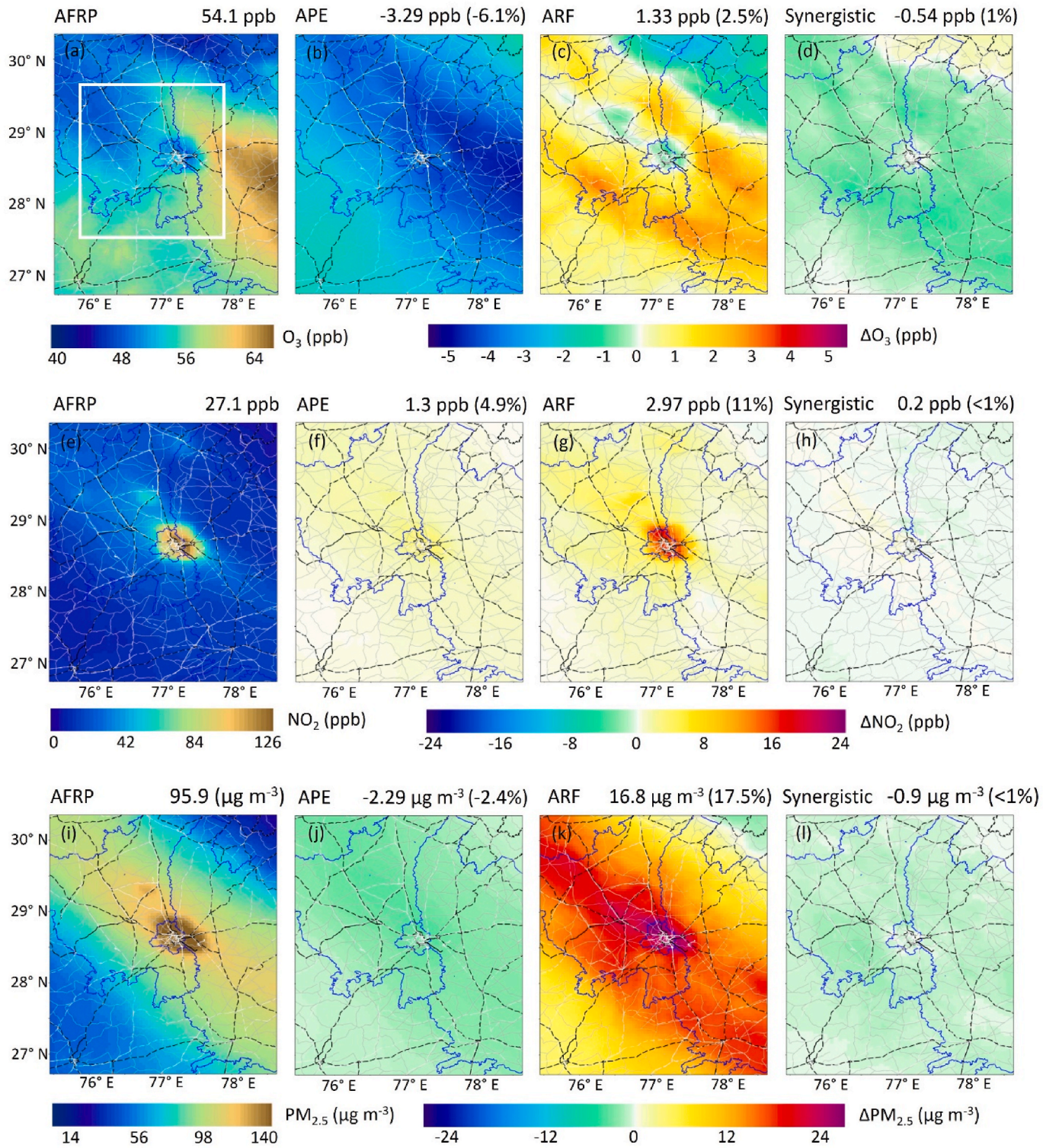

Fig. 3. Spatial distribution of the monthly mean concentrations and changes of O_3 (upper panel), NO_2 (middle panel), and $PM_{2.5}$ (lower panel) averaged during the daytime (07:30–17:30 LT) in November 2018. (**a, e, i)** are from AFRP simulation; **(b, f, j)** are the change of concentrations due to pure APE, **(c, g, k)** are similar to (b, f, j) but due to pure ARF, and (**d, h, l)** are the changes due to synergistic APE and ARF. The calculated values averaged over NCR Delhi (denoted as white box panel (a)) are shown at the top of each panel.

(5.9%), 1.6 μg m^{-3} (4%) and 0.56 μg m^{-3} (4.2%), respectively. The lower abundances of atmospheric oxidants due to the modification of photolysis by pure APE decreases the rate of SNA formation and subsequently alleviates the $PM_{2.5}$ concentrations near the surface.

3.3. Synergistic contribution of APE and ARF

The synergistic impact includes the mutual interactions between the APE and ARF. The synergistic contribution of APE and ARF results in an overall decrease of −0.54 ppb (1%) in the monthly mean O_3 concentration averaged during the daytime (07:30–17:30 LT) (Fig. 3d). In the

Table 2
Pure and synergistic contributions of APE and ARF on O_3, $PM_{2.5}$, NO_2, SNA, photolysis rates, and OH radical concentration.

Contribution	O_3 (ppb)	$PM_{2.5}$ (μg m^{-3})	NO_2 (ppb)	Sulfate (μg m^{-3})	Nitrate (μg m^{-3})	Ammonium (μg m^{-3})	$J[NO_2]$ (10^{-3} s^{-1})	$J[O^1D]$ (10^{-6} s^{-1})	OH (ppt)
AFRP	54.110	95.900	27.140	4.258	40.175	13.290	3.898	9.519	0.075
Pure ARF	1.330	16.770	2.970	0.260	10.397	3.118	0.003	−0.084	−0.007
Pure APE	−3.290	−2.290	1.300	−0.250	−1.600	−0.558	−0.872	−2.260	−0.024
Synergistic APE & ARF	−0.540	−0.890	0.200	−0.029	−0.640	−0.197	−0.024	−0.044	−0.001

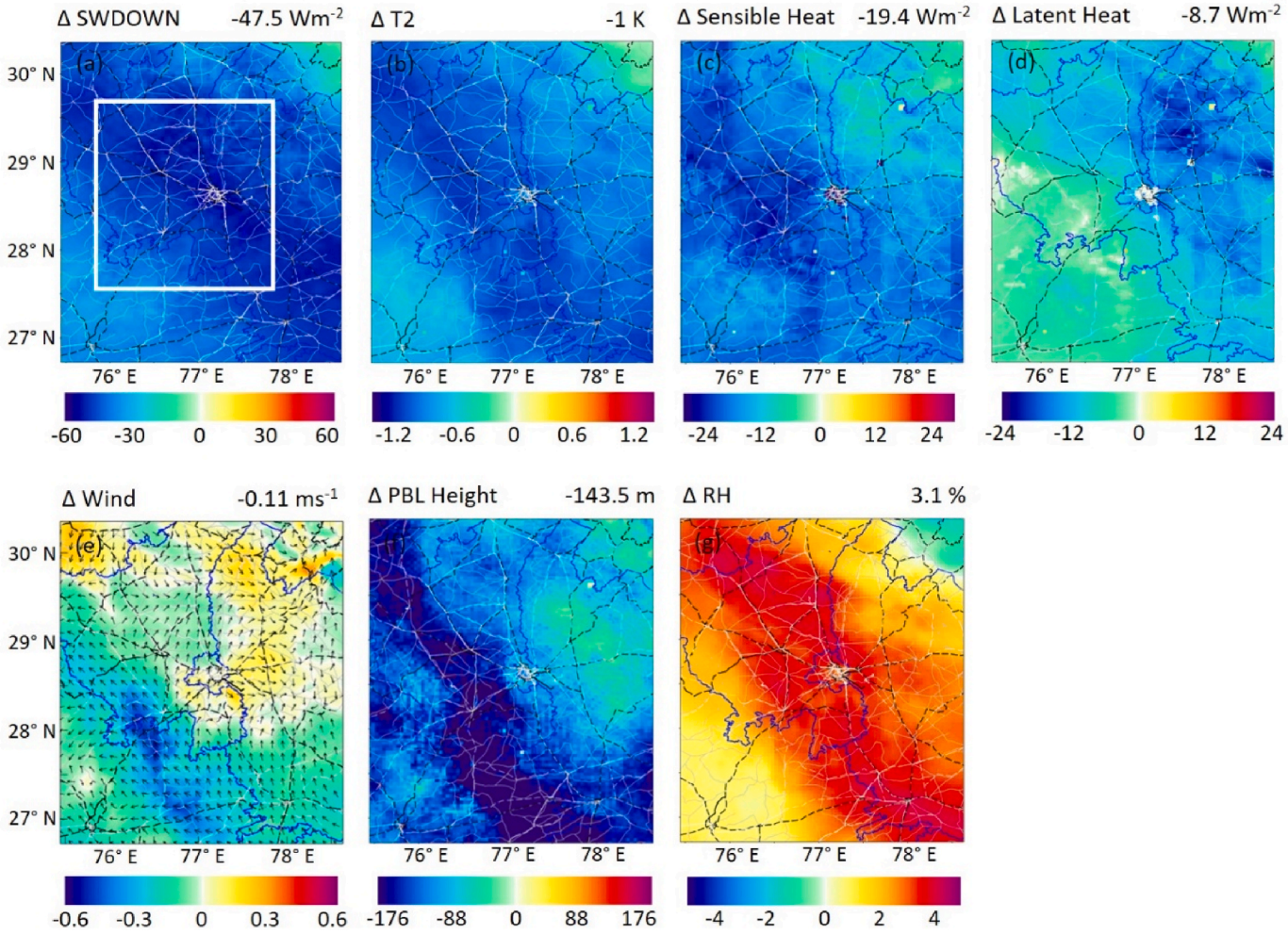

Fig. 4. Changes in the **(a)** downward shortwave (SW) irradiance (Wm^{-2}), **(b)** 2m temperature (K), **(c)** sensible heat (Wm^{-2}), **(d)** latent heat (Wm^{-2}), **(e)** surface wind (ms^{-1}), **(f)** PBL height (m), and **(g)** relative humidity (%), caused by pure ARF during the daytime (07:30–17:30 LT) in November 2018. Shown on the top of each panel are the values averaged over NCR Delhi (denoted as the white box in the top left panel).

case of daily peak (13:30–16:30 LT) O_3, the synergistic APE and ARF contributed −0.8 ppb of total concentration (Fig. S4d). However, in VOC-limited regimes such as in megacity Delhi, the synergistic impact is nearly insignificant (<0.5%) (Fig. 3d and S4d). Similarly, synergistic APE and ARF have a negligible effect on modifying the photolysis rates (<0.5%) (Figs. S1c and f) and consequently little impact on the OH radical (1%) (Fig. S1i) and secondary particulate concentration (<2%) (Figs. S3d, h, l). In the case of NO_2 and $PM_{2.5}$, the synergistic impact contributed less than ±1 % of the total concentrations (Fig. 3h and l). Overall, the synergistic impact of APE and ARF on O_3 and $PM_{2.5}$ concentrations is nearly negligible and far less significant than pure APE and ARF impact.

3.4. Impact of ARF and APE from fire emissions

The mean distribution of $PM_{2.5}$ and O_3 and their precursors due to fire emissions over NCR Delhi during November 2018 is presented in Figs. S5 and 6. Smoke burning enhances the monthly $PM_{2.5}$ concentrations ranging from 1 to 12 μg m^{-3} (daily values up to 10%, Fig. S7), with an average contribution of 4% over the simulated domain (Fig. S5). BC and primary organic aerosol (POA) contributions from fire emissions are 6% and 15%, respectively. An enhancement of 1–3% in the secondary inorganic aerosols is also simulated due to fire emissions (Figs. S5d, e, f). Fire emissions enhance the surface CO concentration up to 65 ppb (14%) over the simulated domain (Fig. S6b). Large enhancement in the gas and aerosol concentrations due to fire is found over the north-western states of Punjab and Haryana where crop residue burning is more intense

during the late autumn, which then are transported in the downwind directions covering NCR Delhi. In monthly average, the ARF from smoke enhances the $PM_{2.5}$, BC, and POA concentrations by 8%, 10%, and 18%, respectively (Fig. 5). ARF contributes 5–7% enhancement in the secondary inorganic aerosol concentrations (Fig. S8). The ARF contributions from the fire emissions show an overall enhancement of 5 ppb in surface CO and 0.1 ppb in surface O_3 concentration in the simulated domain (Fig. 5a and b). Aerosols from fire emissions decrease the shortwave radiation reaching the surface up to 10 Wm^{-2} and temperature up to 0.1 K and increase the relative humidity (Fig. S9). On the other hand, APE from fire results in a 6% reduction in the surface O_3 concentration which is attributed to the lower photolysis rate (Fig. S10), and less than 2% reduction in surface $PM_{2.5}$.

3.5. Discussions

Fig. 6 summarizes the different pathways of APE and ARF affecting O_3 and $PM_{2.5}$. The ARF cools the surface, reduces turbulent mixing, and is conducive to the increase of relative humidity (Fig. 4g), all of which are contributory to the enhancement in surface $PM_{2.5}$ and precursor gas concentration. The enhanced chemical loss via strong NO titration effect ($NO + O_3 \rightarrow NO_2 + O_2$) associated with the high NOx emissions plays a critical role in weakening O_3 production in the megacity Delhi.

In the case of pure APE, the weakening O_3 and OH concentration further impedes the secondary aerosol formations and subsequently alleviates the near-surface $PM_{2.5}$ concentrations. A substantial reduction (~23%) in surface $J[NO_2]$ due to APE has been observed in Beijing, China during haze events further hindering the secondary aerosols (3.5–9.4%) and $PM_{2.5}$ (4.2%) concentrations (Wu et al., 2020), which is consistent with our results. The pure contributions of APE and ARF on surface O_3 as a function of $PM_{2.5}$ in megacity Delhi (Fig. S11) further show that the extent of O_3 changes due to APE is larger than that due to ARF. The APE-induced O_3 reduction is higher when surface $PM_{2.5}$ can reach high levels larger than 180 μg m^{-3} (Fig. S11). Relatively strong APE effects on the surface O_3 formation compared to ARF have also been reported in North China (Yang et al., 2022); however, the synergistic effects were not quantified in their study. Despite the little impact of synergistic APE and ARF effects observed in our study, these findings help to advance our understanding of the complex interactions between aerosol, radiation, and photolysis interactions.

Overall, the elucidation of the role of APE and ARF shows the importance of adopting a comprehensive mitigation strategy to co-control both O_3 and $PM_{2.5}$ concentrations in the megacity Delhi. A combined approach that considers both APE and ARF is important as

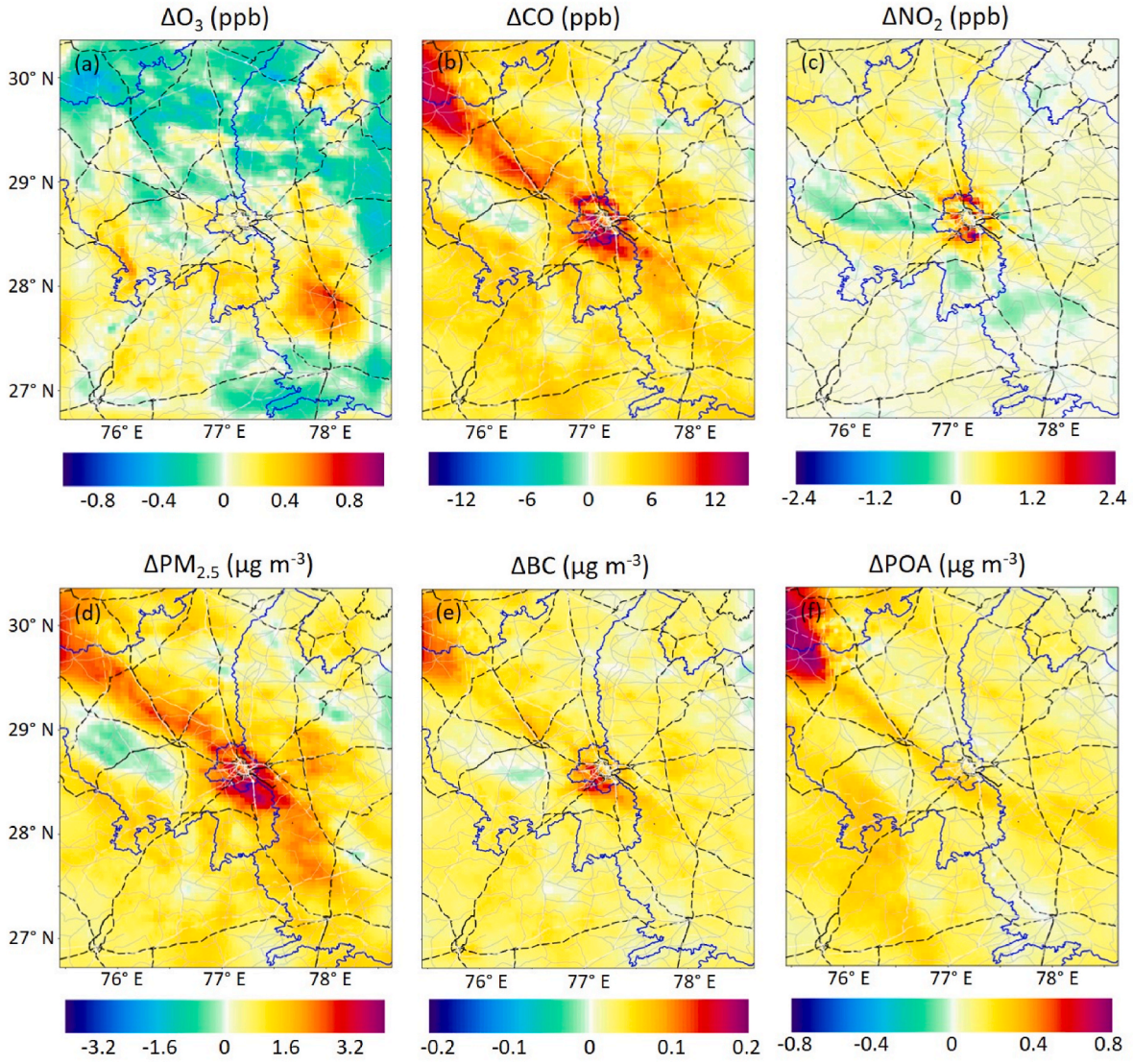

Fig. 5. Spatial distribution of the contributions of ARF from fire emissions on **(a)** O_3, **(b)** CO, **(c)** NO_2 **(d)** $PM_{2.5}$ **(e)** BC, and **(f)** POA averaged during the daytime (07:30–17:30 LT) in November 2018.

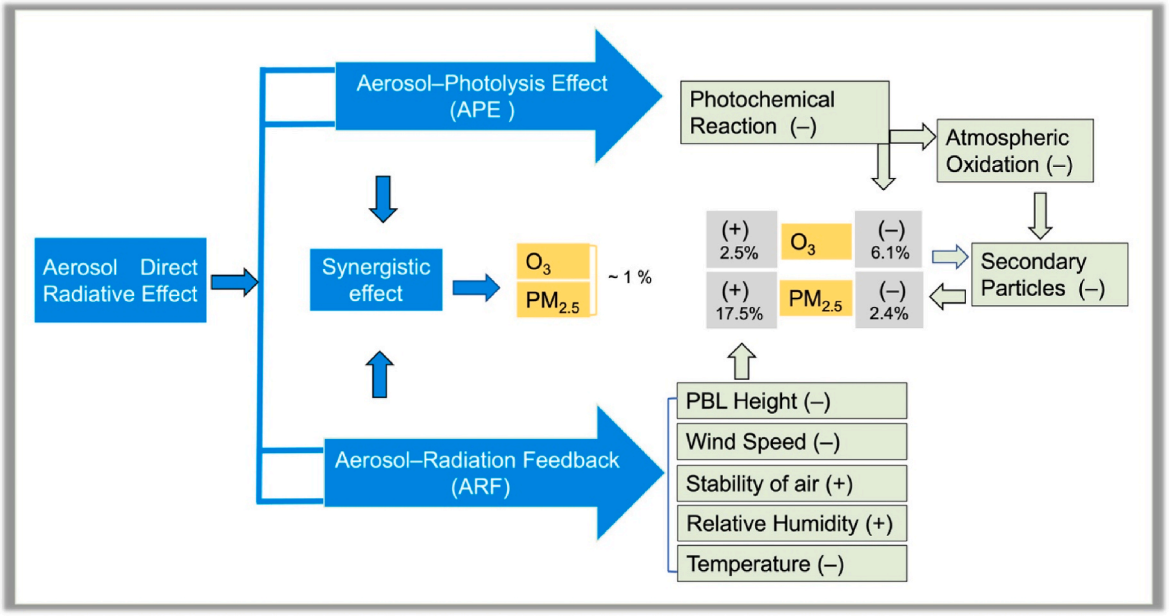

Fig. 6. Different pathways showing APE and ARF effects on $PM_{2.5}$ and O_3. The '+' and '–' signs denote increasing and decreasing effects, respectively.

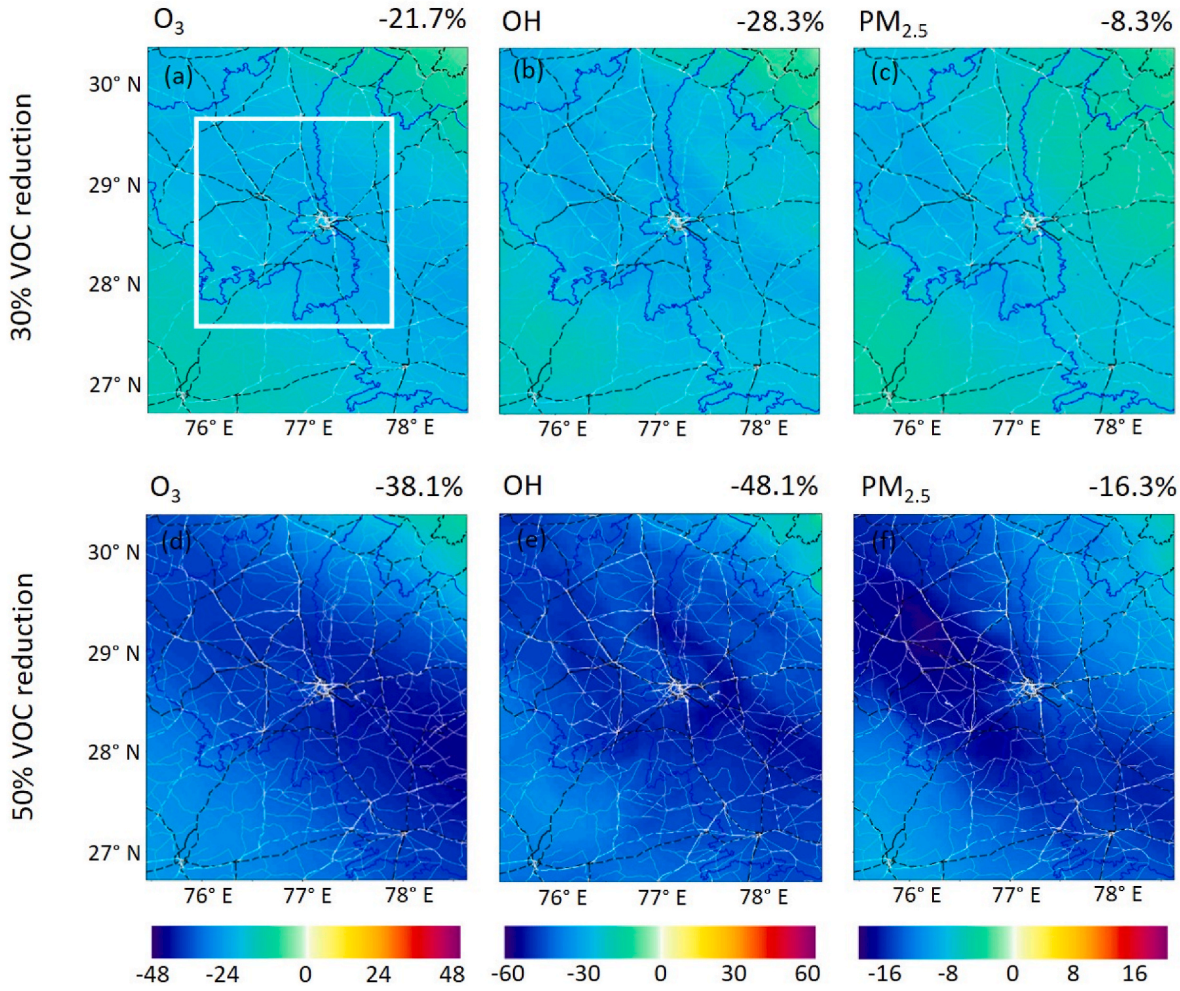

Fig. 7. (a, d) O_3 **(b, e)** OH and **(c, f)** $PM_{2.5}$ responses to the 30% and 50% reduction of VOC emissions over NCR Delhi in November 2018.

neglecting either factor could lead to unexpected consequences for the other pollutant. For example, controlling $PM_{2.5}$ concentration by reducing emissions may lead to O_3 escalation by increasing photolysis and at the same time reduce O_3 by increasing the solar input at the surface and hence, the turbulent mixing. Since surface O_3 formation in Delhi is VOC limited and VOCs are common precursors for both O_3 and $PM_{2.5}$, effective control of VOC emissions is required to counterbalance future O_3 escalations.

To examine the O_3 and $PM_{2.5}$ responses to VOC emission reduction, we have performed two more sensitivity experiments by reducing VOC anthropogenic emissions by 30% and 50% (Figure S12 and Fig. 7) with fire emissions turned on and accounting both APE and ARF effects. This integrated approach has significant importance, as biomass burning emissions also contribute to VOC emissions, with CO being one such component that is considered in this study. The 30% VOC reduction resulted in a decrease of surface O_3 concentration by 21% over NCR Delhi (Fig. 7a). The O_3 decrease became 38% in the 50% VOC emission reduction scenario and led to a large decrease (48%) in the OH radical concentration (Fig. 7d and e). As OH is the key reactive species in the formation of secondary inorganic aerosols, the reduction in VOC emissions by 30–50% reduces the SNA concentration by 12–26% (Fig. S13). As a result, the 30% and 50% reduction of VOC leads to a decrease in $PM_{2.5}$ concentration by 8% and 16%, respectively (Fig. 7c–f). Our study suggests that controlling VOC emissions effectively helps in lowering O_3 levels directly and also indirectly via weakening ARF effects from the reduced $PM_{2.5}$, emphasizing the need and efficacy of VOC control for simultaneous mitigation of O_3 and $PM_{2.5}$ in Delhi. Additionally, considering the notable influence of APE and ARF from fire emissions, it is imperative to comprehensively account for the contribution of crop residue burning to the pollution levels and their transport processes across the northern Indian region in the air quality mitigation efforts.

In our study, we explored how APE and ARF influence surface O_3 and $PM_{2.5}$ levels within the same fire and anthropogenic emission inventories and chemical mechanism. While the choice of emission inventories (including fire and anthropogenic) and chemical mechanisms can significantly influence the magnitude of these effects on O_3 and $PM_{2.5}$, our key findings remain consistent across different inventories. We conducted a comparative analysis for $PM_{2.5}$ emissions from multiple inventories, such as HTAPv2 (Janssens-Maenhout et al., 2015), EDGARv5 (Crippa et al., 2021), and the latest HTAPv3 (Crippa et al., 2023) with detailed sectoral disaggregation. Notable differences were observed over the Indian region (see Fig. S14), specifically, over mainland India, HTAPv2 emissions exceeded EDGARv5 by 14% and HTAPv3 by 13%, while in the NCR Delhi, HTAPv2 emissions were 30% higher than HTAPv3 and exhibited similar performance to EDGARv5 (Fig. S14). The monthly averaged diurnal variation plot between observed and model simulated $PM_{2.5}$ concentrations using both HTAPv2 and HTAPv3 revealed an overall normalized mean bias (NMB) of 36.8% for HTAPv3 and 2% for HTAPv2 in megacity Delhi during November 2018 (Fig. S15c). While there are variations in the magnitude of observed effects with different inventories, the overall direction of the impacts remains consistent across different emission inventories. Model results using both HTAPv2 and HTAPv3 inventory showed significant impact on $PM_{2.5}$ levels due to emissions, although differences in absolute values. Nevertheless, the relative differences remained similar across different inventories. Regardless of the inventory used, our key findings regarding the contribution of APE to the reduction in surface O_3 and $PM_{2.5}$ concentrations and the role of urban VOC control in reducing both O_3 and $PM_{2.5}$ remain unchanged. Additionally, the synergistic impact of APE and ARF on O_3 and $PM_{2.5}$ concentrations is less significant than their individual impacts, irrespective of the emission inventory employed. We focused on HTAPv2 for this study as the model simulated chemical variables using HTAPv2 compared well with observed data and showed better agreement than HTAPv3 in our analysis. In our future work, we plan to explore how the absolute values of observed effects change with different emission inventories (fire and anthropogenic) and chemical mechanisms and to consider additional emission sources, such as open waste burning (Sharma et al., 2019) and fine-tune the latest HTAPv3 based on regional inventory data over Indian region.

Moreover, we intend to focus on latest Fire Inventory from NCAR version 2.5 (FINNv2.5) emission inventory (Wiedinmyer et al., 2023), which employs both MODIS and VIIRS-based fire counts, and provides VOC species for various chemical mechanisms, including MOZART, GEOS-Chem, and SAPRC99, resulting in substantially higher fire emissions compared to FLAMBE (See Fig. S16) and FINNv1.5 (Wiedinmyer et al., 2023). Previous studies by Zhang et al. (2014) also found significant differences among smoke inventories, with FLAMBE showing the largest emissions in tropical Africa. These comparisons highlight the need for a comprehensive evaluation of fire emissions. While differences in emissions between FLAMBE and FINNv2.5 affect the magnitude of the fire impact, the main findings of our work remain consistent across different emission inventories, similar to cases involving anthropogenic emissions. For instance, reducing VOC emissions (e.g., by 50%) leads to a decrease in oxidant levels (O_3 and OH) and secondary aerosols, resulting in a reduction in $PM_{2.5}$, regardless of the emission inventory used. To provide a more comprehensive assessment of emission effects, especially for understanding VOC emissions, we plan to expand our analysis by mapping non-methane organic compounds (NMOC) emissions to the RADM2 chemical mechanism for FINNv2.5.

4. Summary and conclusions

The pure and synergistic impacts of APE and ARF on surface O_3 and $PM_{2.5}$ are quantified using a regional model UI-WRF-Chem employing the FSA method over NCR Delhi in November 2018. The model performance in simulating surface O_3 and $PM_{2.5}$ is improved after the inclusion of both APE and ARF with a significant reduction in mean bias in the megacity Delhi. The results reveal that APE reduces the surface O_3 and $PM_{2.5}$ concentrations by 6.1% and 2.4%, respectively over NCR Delhi. On the other hand, the increased atmospheric stability due to ARF hinders the pollutant's outflow and enhances the $PM_{2.5}$ (17.5%) and O_3 (2.5%) concentrations. The synergistic APE and ARF contributed very little (~1%) to the surface O_3 and $PM_{2.5}$ concentration. The ARF deteriorates the air quality during the crop residue burning period, enhancing the monthly average $PM_{2.5}$, BC, and POA concentrations by 8%, 10%, and 18%, respectively. This study implies that reducing $PM_{2.5}$ concentrations may lead to O_3 escalation due to weakened aerosol radiation interactions. Considering the remarkable impact of APE and ARF on O_3 and $PM_{2.5}$, these effects need to be considered in designing policies for co-controlling O_3 and $PM_{2.5}$. Reducing VOC emissions (by 50%) results in a decrease in the oxidant levels (38–48% decrease in O_3 and OH) and secondary aerosols (22–26%) and leads to a 16% $PM_{2.5}$ reduction, highlighting the effectiveness of VOC control in achieving O_3 and $PM_{2.5}$ reductions in Delhi. Furthermore, in light of the significant influence of APE and ARF from fire, it becomes crucial to consider both pollution sources and transport processes across the Indian subcontinent when implementing air quality mitigation strategies.

This study provides first-hand information on evaluating the effects of APE and ARF on O_3 and $PM_{2.5}$ using a meteorology–chemistry modeling framework in Delhi. The elucidation of the role of APE and ARF is particularly significant in understanding the complex $PM_{2.5} - O_3$ nexus over polluted regions and the co-benefits attributed to the reduction in both pollutants. However, other factors such as heterogeneous reactions associated with aerosol and aerosol-cloud interactions also need to be considered for further insights into the impact of aerosol radiative effects on O_3 and $PM_{2.5}$ concentration. Furthermore, expanding the systematic observations of aerosol composition and optical properties in the study region along with development of up-to-date time varying regional inventories can lead to a more comprehensive evaluation of aerosol radiative effects and their contribution to the regional climate dynamics. Future research will explore how the absolute values of observed effects vary with different emission inventories

(fire and anthropogenic) and chemical mechanisms, while also considering additional emission sources such as open waste burning and fine-tuning global inventories based on regional inventory data over Indian region.

CRediT authorship contribution statement

Lakhima Chutia: Writing – review & editing, Writing – original draft, Visualization, Validation, Software, Methodology, Investigation, Formal analysis, Data curation, Conceptualization. **Jun Wang:** Writing – review & editing, Supervision, Project administration, Methodology, Funding acquisition, Conceptualization. **Huanxin Zhang:** Formal analysis, Data curation. **Xi Chen:** Data curation. **Lorena Castro Garcia:** Visualization, Data curation. **Nathan Janechek:** Data curation.

Data availability statement

The Central Pollution Control Board (CPCB) of India dataset (for $PM_{2.5}$, O_3, T2, and RH) is available at https://app.cpcbccr.com/ccr/#/caaqm-dashboard-all/caaqm-landing. WRF-Chem is an open-access model which can be acquired at https://www2.acom.ucar.edu/wrf-chem. The authors thank NASA for making MERRA-2 reanalysis (https://gmao.gsfc.nasa.gov/reanalysis/MERRA-2/) and GLDAS (https://disc.gsfc.nasa.gov/datasets?keywords=GLDAS) data publicly accessible. The EDGAR-HTAP v2 anthropogenic emissions were obtained from https://edgar.jrc.ec.europa.eu/dataset_htap_v2.

Declaration of competing interest

The authors declare that they have no known competing financial interests or personal relationships that could have appeared to influence the work reported in this paper.

Acknowledgments

We sincerely thank NASA Atmospheric Composition Modeling and Analysis Program (ACMAP, award number 80NSSC19K0950) and Multi-Angle Imager for Aerosols (MAIA, award number: H389700) satellite mission for funding this research. The authors acknowledge the High-Performance Computing at the University of Iowa for model simulations.

Appendix A. Supplementary data

Supplementary data to this article can be found online at https://doi.org/10.1016/j.atmosenv.2024.120890.

Data availability

Data will be made available on request.

References

Bawase, M., Sathe, Y., Khandaskar, H., Sukrut, T., 2021. Chemical composition and source attribution of $PM_{2.5}$ and PM_{10} in Delhi-National Capital Region (NCR) of India: results from an extensive seasonal campaign. J. Atmos. Chem. 78, 35–58. https://doi.org/10.1007/s10874-020-09412-7.

Benas, N., Mourtzanou, E., Kouvarakis, G., Bais, A., Mihalopoulos, N., Vardavas, I., 2013. Surface ozone photolysis rate trends in the Eastern Mediterranean: modeling the effects of aerosols and total column ozone based on Terra MODIS data. Atmos. Environ. 74, 1–9. https://doi.org/10.1016/j.atmosenv.2013.03.019.

Bharali, C., Nair, V.S., Chutia, L., Babu, S., 2019. Modeling of the effects of wintertime aerosols on boundary layer properties over the indo gangetic plain. J. Geophys. Res. Atmos. 124. https://doi.org/10.1029/2018JD029758.

Bhuvaneshwari, S., Hettiarachchi, H., Meegoda, J.N., 2019. Crop residue burning in India: policy challenges and potential solutions. Int J Environ Res Public Health 16 (5), 832. https://doi.org/10.3390/ijerph16050832. PMID: 30866483; PMCID: PMC6427124.

Bran, S.H., Srivastava, R., 2017. Investigation of PM(2.5) mass concentration over India using a regional climate model. Environ Pollut 224, 484–493. https://doi.org/10.1016/j.envpol.2017.02.030.

Chou, M.-D., Suarez, M.J., 1994. An efficient thermal infrared radiation parameterization for use in general circulation models. NASA Technical Memorandum 104606 3, 85. https://archive.org/details/nasa_techdoc_19950009331.

Chutia, L., Ojha, N., Girach, I.A., Sahu, L.K., Alvarado, L.M.A., Burrows, J.P., Pathak, B., Bhuyan, P.K., 2019. Distribution of volatile organic compounds over Indian subcontinent during winter: WRF-chem simulation versus observations. Environ Pollut 252 (Pt A), 256–269. https://doi.org/10.1016/j.envpol.2019.05.097.

Conibear, L., Butt, E.W., Knote, C., Arnold, S.R., Spracklen, D.V., 2018. Residential energy use emissions dominate health impacts from exposure to ambient particulate matter in India. Nat. Commun. 9 (1), 617. https://doi.org/10.1038/s41467-018-02986-7.

CPCB (Central Pollution Control Board), 2018. Guidelines for Continuous Emission Monitoring Systems. Revision-I.

Crippa, M., Guizzardi, D., Butler, T., Keating, T., Wu, R., Kaminski, J., Kuenen, J., Kurokawa, J., Chatani, S., Morikawa, T., Pouliot, G., Racine, J., Moran, M.D., Klimont, Z., Manseau, P.M., Mashayekhi, R., Henderson, B.H., Smith, S.J., Suchyta, H., Muntean, M., Solazzo, E., Banja, M., Schaaf, E., Pagani, F., Woo, J.-H., Kim, J., Monforti-Ferrario, F., Pisoni, E., Zhang, J., Niemi, D., Sassi, M., Ansari, T., Foley, K., 2023. The HTAP_v3 emission mosaic: merging regional and global monthly emissions (2000–2018) to support air quality modelling and policies. Earth Syst. Sci. Data 15, 2667–2694. https://doi.org/10.5194/essd-15-2667-2023.

Crippa, M., Guizzardi, D., Muntean, M., Schaaf, E., 2021. EDGAR v5.0 Global Air Pollutant Emissions, vol. 2021. European Commission, JRC122516.

Fast, J.D., Gustafson, W.I., Easter, R.C., Zaveri, R.A., Barnard, J.C., Chapman, E.G., Grell, G.A., Peckham, S.E., 2006. Evolution of ozone, particulates, and aerosol direct radiative forcing in the vicinity of Houston using a fully coupled meteorology chemistry-aerosol model. J. Geophys. Res. Atmos. 111, D21305. https://doi.org/10.1029/2005JD006721.

Flynn, J., Lefer, B., Rappenglück, B., Leuchner, M., Perna, R., Dibb, J., Crawford, J., 2010. Impact of clouds and aerosols on ozone production in Southeast Texas. Atmos. Environ. 44 (33), 4126–4133. https://doi.org/10.1016/j.atmosenv.2009.09.005.

Ge, C., Wang, J., Reid, J.S., Posselt, D.J., Xian, P., Hyer, E.J., 2017. Mesoscale modeling of smoke transport from equatorial Southeast Asian Maritime Continent to the Philippines: first comparison of ensemble analysis with in situ observations. J. Geophys. Res. 122, 5380–5398.

Ghude, S.D., Chate, D.M., Jena, C., Beig, G., Kumar, R., Barth, M.C., Pithani, P., 2016. Premature mortality in India due to PM2.5 and ozone exposure. Geophys. Res. Lett. 43 (9), 4650–4658. https://doi.org/10.1002/2016GL068949.

Girach, I.A., Ojha, N., Nair, P.R., Pozzer, A., Tiwari, Y.K., Kumar, K.R., Lelieveld, J., 2017. Variations in O3, CO, and CH4 over the Bay of Bengal during the summer monsoon season: shipborne measurements and model simulations. Atmos. Chem. Phys. 17, 257–275. https://doi.org/10.5194/acp-17-257-2017.

Grell, G.A., Peckham, S.E., Schmitz, R., McKeen, S.A., Frost, G., Skamarock, W.C., Eder, B., 2005. Fully coupled "online" chemistry within the WRF model. Atmos. Environ. 39 (37), 6957–6975.

Hakim, Z.Q., Archer-Nicholls, S., Beig, G., Folberth, G.A., Sudo, K., Abraham, N.L., Archibald, A.T., 2019. Evaluation of tropospheric ozone and ozone precursors in simulations from the HTAPII and CCMI model intercomparisons – a focus on the Indian subcontinent. Atmos. Chem. Phys. 19 (9), 6437–6458. https://doi.org/10.5194/acp-19-6437-2019.

Janssens-Maenhout, G., Crippa, M., Guizzardi, D., Dentener, F., Muntean, M., Pouliot, G., Li, M., 2015. HTAP_v2.2: a mosaic of regional and global emission grid maps for 2008 and 2010 to study hemispheric transport of air pollution. Atmos. Chem. Phys. 15 (19), 11411–11432. https://doi.org/10.5194/acp-15-11411-2015.

Jat, R., Gurjar, B.R., Lowe, D., 2021. Regional pollution loading in winter months over India using high resolution WRF-Chem simulation. Atmos. Res. 249, 105326. https://doi.org/10.1016/j.atmosres.2020.105326.

Kumar, R., Ghude, S.D., Biswas, M., Jena, C., Alessandrini, S., Debnath, S., Rajeevan, M., 2020. Enhancing accuracy of air quality and temperature forecasts during paddy crop residue burning season in Delhi via chemical data assimilation. J. Geophys. Res. Atmos. 125 (17), e2020JD033019. https://doi.org/10.1029/2020JD033019.

Lan, R., Eastham, S.D., Liu, T., Norford, L.K., Barrett, S.R.H., 2022. Air quality impacts of crop residue burning in India and mitigation alternatives, 13 Nat. Commun. 14 (1), 6537. https://doi.org/10.1038/s41467-022-34093-z. PMID: 36376316; PMCID: PMC.

Li, G., Bei, N., Tie, X., Molina, L.T., 2011. Aerosol effects on the photochemistry in Mexico City during MCMA-2006/MILAGRO campaign. Atmos. Chem. Phys. 11 (11), 5169–5182. https://doi.org/10.5194/acp-11-5169-2011.

Li, G., Zhang, R., Fan, J., Tie, X., 2005. Impacts of black carbon aerosol on photolysis and ozone. J. Geophys. Res. Atmos. 110 (D23).

Liao, H., Yung, Y., Seinfeld, J., 1999. Effect of aerosols on tropospheric photolysis rates in clear and cloudy atmospheres. J. Geophys. Res. 1042, 23697–23708. https://doi.org/10.1029/1999JD900409.

Liu, Q., Jia, X., Quan, J., Li, J., Li, X., Wu, Y., Liu, Y., 2018. New positive feedback mechanism between boundary layer meteorology and secondary aerosol formation during severe haze events. Sci. Rep. 8 (1), 6095. https://doi.org/10.1038/s41598-018-24366-3.

Mogno, C., Palmer, P.I., Knote, C., Yao, F., Wallington, T.J., 2021. Seasonal distribution and drivers of surface fine particulate matter and organic aerosol over the Indo-Gangetic Plain. Atmos. Chem. Phys. 21 (14), 10881–10909. https://doi.org/10.5194/acp-21-10881-2021.

Mukherjee, T., Vinoj, V., Midya, S.K., Puppala, S.P., Adhikary, B., 2020. Numerical simulations of different sectoral contributions to post monsoon pollution over Delhi. Heliyon 6 (3), e03548. https://doi.org/10.1016/j.heliyon.2020.e03548.

Nelson, B.S., Stewart, G.J., Drysdale, W.S., Newland, M.J., Vaughan, A.R., Dunmore, R. E., Lee, J.D., 2021. In situ ozone production is highly sensitive to volatile organic compounds in Delhi, India. Atmos. Chem. Phys. 21 (17), 13609–13630. https://doi.org/10.5194/acp-21-13609-2021.

Ojha, N., Sharma, A., Kumar, M., Girach, I., Ansari, T.U., Sharma, S.K., Gunthe, S.S., 2020. On the widespread enhancement in fine particulate matter across the Indo-Gangetic Plain towards winter. Sci. Rep. 10 (1), 5862. https://doi.org/10.1038/s41598-020-62710-8.

Real, E., Sartelet, K., 2011. Modeling of photolysis rates over Europe: impact on chemical gaseous species and aerosols. Atmos. Chem. Phys. 11 (4), 1711–1727. https://doi.org/10.5194/acp-11-1711-2011.

Reid, J.S., Hyer, E.J., Prins, E.M., Westphal, D.L., Zhang, J., Wang, J., Hoffman, J.P., 2009. Global monitoring and forecasting of biomass-burning smoke: description of and lessons from the fire locating and modeling of burning emissions (FLAMBE) Program. IEEE J. Sel. Top. Appl. Earth Obs. Rem. Sens. 2 (3), 144–162. https://doi.org/10.1109/JSTARS.2009.2027443.

Sahu, S.K., Kota, S.H., 2017. Significance of PM2.5 air quality at the Indian capital. Aerosol Air Qual. Res. 17 (2), 588–597. https://doi.org/10.4209/aaqr.2016.06.0262.

Saxena, P., Sonwani, S., Srivastava, A., Jain, M., Srivastava, A., Bharti, A., Rangra, D., Mongia, N., Tejan, S., Bhardwaj, S., 2021. Impact of crop residue burning in Haryana on the air quality of Delhi, India. Heliyon 2021, e06973. https://doi.org/10.1016/j.heliyon.2021.e06973.

Schell, B., Ackermann, I.J., Hass, H., Binkowski, F.S., Ebel, A., 2001. Modeling the formation of secondary organic aerosol within a comprehensive air quality model system. J. Geophys. Res. Atmos. 106 (D22), 28275–28293.

Sha, T., Ma, X., Zhang, H., Janechek, N., Wang, Y., Wang, Y., Wang, J., 2021. Impacts of soil NOx emission on O3 air quality in rural California. Environ. Sci. Technol. 55 (10), 7113–7122. https://doi.org/10.1021/acs.est.0c06834.

Sharma, G., Sinha, B., Hakkim, H., Chandra, B.P., Kumar, A., Sinha, B., 2019. Gridded emissions of CO, NOx, SO2, CO2, NH3, HCl, CH4, PM2.5, PM10, BC, and NMVOC from open municipal waste burning in India. Environ. Sci. Technol. 53 (9), 4765–4774. https://doi.org/10.1021/acs.est.8b07076.

Sharma, A., Ojha, N., Pozzer, A., Mar, K.A., Beig, G., Lelieveld, J., Gunthe, S.S., 2017. WRF-Chem simulated surface ozone over south Asia during the pre-monsoon: effects of emission inventories and chemical mechanisms. Atmos. Chem. Phys. 17 (23), 14393–14413. https://doi.org/10.5194/acp-17-14393-2017.

Singh, A., Srivastava, A.K., Varaprasad, V., Kumar, V., Pathak, V., Shukla, A.K., 2021. Assessment of near-surface air pollutants at an urban station over the central Indo-Gangetic Basin: role of pollution transport pathways. Meteorol. Atmos. Phys. 133, 1127–1142. https://doi.org/10.1007/s00703-021-00798-x.

Singh, A., Vishnoi, A.S., Banday, A.H., Bora, P., Paney, P., 2023. Influence of stubble burning on air quality of Northern India: a case study of Indo-Gangetic plains of India. Environ. Monit. Assess. 195, 487. https://doi.org/10.1007/s10661-023-11027-w.

Sinha, B., Singh Sangwan, K., Maurya, Y., Kumar, V., Sarkar, C., Chandra, B.P., Sinha, V., 2015. Assessment of crop yield losses in Punjab and Haryana using 2 years of continuous in situ ozone measurements. Atmos. Chem. Phys. 15 (16), 9555–9576. https://doi.org/10.5194/acp-15-9555-2015.

Stein, U., Alpert, P., 1993. Factor separation in numerical simulations. J. Atmos. Sci. 50 (14), 2107–2115. https://doi.org/10.1175/1520-0469(1993)050<2107:Fsins>2.0.Co;2.

Stockwell, W.R., Middleton, P., Chang, J.S., Tang, X., 1990. The second generation regional acid deposition model chemical mechanism for regional air quality modeling. J. Geophys. Res. Atmos. 95 (D10), 16343–16367.

Tie, X., Madronich, S., Walters, S., Zhang, R., Rasch, P., Collins, W., 2003. Effect of clouds on photolysis and oxidants in the troposphere. J. Geophys. Res. Atmos. 108 (D20). https://doi.org/10.1029/2003JD003659.

Wang, J., Ge, C., Yang, Z., Hyer, E.J., Reid, J.S., Chew, B.-N., Zhang, M., 2013. Mesoscale modeling of smoke transport over the Southeast Asian Maritime Continent: interplay of sea breeze, trade wind, typhoon, and topography. Atmos. Res. 122, 486–503. https://doi.org/10.1016/j.atmosres.2012.05.009.

Wang, Y., Wang, J., Zhang, H., Janechek, N., Wang, Y., Zhou, M., Shen, P., Tan, J., He, Q., Cheng, T., Cheng, C., 2023. Impact of land use change on the urban-rural disparity of summer temperature in Eastern China. Atmos. Environ. 308, 119850.

Wang, Y., Yu, M., Wang, Y., Tang, G., Song, T., Zhou, P., Petäjä, T., 2020. Rapid formation of intense haze episodes via aerosol–boundary layer feedback in Beijing. Atmos. Chem. Phys. 20 (1), 45–53. https://doi.org/10.5194/acp-20-45-2020.

World Health Organization, 2021. WHO global air quality guidelines (2021). Particulate Matter (PM2.5 and PM10), Ozone, Nitrogen Dioxide, Sulfur Dioxide and Carbon Monoxide [Internet]. Geneva: World Health Organization; 2021. Available from: https://www.ncbi.nlm.nih.gov/books/NBK574594/.

Wiedinmyer, C., Kimura, Y., McDonald-Buller, E.C., Emmons, L.K., Buchholz, R.R., Tang, W., Seto, K., Joseph, M.B., Barsanti, K.C., Carlton, A.G., Yokelson, R., 2023. The Fire Inventory from NCAR version 2.5: an updated global fire emissions model for climate and chemistry applications. Geosci. Model Dev. (GMD) 16, 3873–3891. https://doi.org/10.5194/gmd-16-3873-2023.

Wu, J., Bei, N., Hu, B., Liu, S., Wang, Y., Shen, Z., Li, G., 2020. Aerosol-photolysis interaction reduces particulate matter during wintertime haze events. Proc Natl Acad Sci U S A 117 (18), 9755–9761. https://doi.org/10.1073/pnas.1916775117.

Xing, J., Wang, J., Mathur, R., Wang, S., Sarwar, G., Pleim, J., Hao, J., 2017. Impacts of aerosol direct effects on tropospheric ozone through changes in atmospheric dynamics and photolysis rates. Atmos. Chem. Phys. 17 (16), 9869–9883. https://doi.org/10.5194/acp-17-9869-2017.

Yang, H., Chen, L., Liao, H., Zhu, J., Wang, W., Li, X., 2022. Impacts of aerosol–photolysis interaction and aerosol–radiation feedback on surface-layer ozone in North China during multi-pollutant air pollution episodes. Atmos. Chem. Phys. 22 (6), 4101–4116. https://doi.org/10.5194/acp-22-4101-2022.

Zhang, F., Wang, J., Ichoku, C., Hyer, E.J., Yang, Z., Ge, C., Su, S., Zhang, X., Kondragunta, S., Kaiser, J.W., 2014. Sensitivity of mesoscale modeling of smoke direct radiative effect to the emission inventory: a case study in northern sub-Saharan African region. Environmental Research Letter 9, 075002. https://doi.org/10.1088/1748-9326/9/7/075002.